Calculating electron cyclotron current drive stabilization of resistive tearing modes in a nonlinear MHD model

Thomas G. Jenkins[a], Scott E. Kruger[b], C. C. Hegna[c], Dalton D. Schnack[a], and Carl R. Sovinec[c]

a) Department of Physics, University of Wisconsin, Madison, Wisconsin, 53706
b) Tech–X Corporation, 5621 Arapahoe Avenue Suite A, Boulder, Colorado, 80303
c) Department of Engineering Physics, University of Wisconsin, Madison, Wisconsin, 53706

Abstract

A model which incorporates the effects of electron cyclotron current drive (ECCD) into the magnetohydrodynamic (MHD) equations is implemented in the NIMROD code [C. R. Sovinec *et al.*, J. Comp. Phys. **195**, 355 (2004)] and used to investigate the effect of ECCD injection on the stability, growth, and dynamical behavior of magnetic islands associated with resistive tearing modes. In addition to qualitatively and quantitatively agreeing with numerical results obtained from the inclusion of localized ECCD deposition in static equilibrium solvers [A. Pletzer and F. W. Perkins, Phys. Plasmas **6**, 1589 (1999)], predictions from the model further elaborate the role which rational surface motion plays in these results. The complete suppression of the $(2, 1)$ resistive tearing mode by ECCD is demonstrated and the relevant stabilization mechanism is determined. Consequences of the shifting of the mode rational surface in response to the injected current are explored, and the characteristic short–time responses of resistive tearing modes to spatial ECCD alignments which are stabilizing are also noted. We discuss the relevance of this work to the development of more comprehensive predictive models for ECCD–based mitigation and control of neoclassical tearing modes.

I Introduction

Tearing modes are slowly growing, nonideal magnetohydrodynamic instabilities which produce magnetic islands at low–order rational surfaces in toroidal plasmas. Neoclassical tearing modes (NTMs) [1, 2] can be triggered by magnetic perturbations which induce a local flattening in the plasma pressure profile. If this flattening is sufficient to suppress the local bootstrap current (which depends on the local pressure gradient), the resulting helical modification to the current profile reinforces the initial magnetic perturbation, yielding magnetic island growth until nonlinear saturation is attained. When present, these modes can slow plasma rotation [3], reduce core electron density and temperature [4, 5], and possibly lead to disruption [6, 7, 8].

While various methods for the mitigation and control of tearing modes have been implemented in existing experiments [9, 10, 11], the most successful has been the use of external current drive to stabilize the magnetic islands. Electron cyclotron current drive has localized deposition [12] which enables the driven currents to both locally modify the equilibrium [13] and compete with the perturbed island currents [14, 15]. Experimental results have successfully demonstrated stabilization on several devices [16, 17, 18, 19, 20]. Sophisticated active feedback control can be used to locate islands and drive time–modulated currents as the island rotates; alternatively, continuously driven current whose spatial alignment is tailored to yield a net stabilizing effect on the NTM may be employed [10, 11, 21, 22, 23, 24].

Although efforts to suppress and/or control NTMs in existing experiments have met with notable success, further developments are needed to remove uncertainties in the scaling of current experimental results to ITER [25, 26, 27, 28]. The development of predictive computational models to simulate the interaction of MHD with ECCD and other forms of RF would help remove these uncertainties, but such simulations remain a significant challenge [29]. In part, this is due to the disparity in the relevant timescales; the Alfvén time characterizing MHD phenomena may vary by orders of magnitude from both the more rapid electron cyclotron period and the slower resistive timescales associated with NTMs. The major difficulty, however, is that kinetic effects, such as RF–modified heat transport and its effect on the pressure profile and bootstrap current [30], are difficult to calculate self-consistently. The conventional method of using a bounce–averaged Fokker–Planck equation to kinetically calculate driven current and heating [31] is insufficient for the calculation of the kinetic distortions that occur in the presence of a three-dimensional island. The best way of calculating these kinetic effects is a subject of ongoing research.

Though a fully-coupled, self–consistent model for ECCD/MHD interaction is not realized in this work, we explore a number of physics issues relevant to this coupling in the context of a theoretical framework [32] which allows such a model. In Section II of this paper, we present the equations that are used and discuss their relevance to the physics we wish to study. In Section III we implement this model in the NIMROD code [33]. An unstable equilibrium is used to investigate current–induced modification of the tearing mode stabil-

ity parameter and the motion of rational surfaces. Rational surface motion is shown to account for and yield greater insight into data obtained by Pletzer and Perkins [13] modeling the stability of Grad–Shafronov equilibria modified by RF currents. Section IV discusses the dynamic response of the plasma to ECCD deposition on shorter timescales, and the competing mechanisms for tearing mode stabilization are analyzed. Finally, Section V summarizes key results and discusses the relevance of this simulation model to the more general problem of simulating ECCD stabilization of NTMs.

II Preliminary ECRF/MHD model

Previous efforts in the numerical modeling of ECCD stabilization in MHD codes can be roughly categorized into two types of simulations. In the first type [34, 35, 36, 37], the current source is given by modifying the resistive Ohm's law,

$$\mathbf{E} + \mathbf{u} \times \mathbf{B} = \frac{\eta}{\mu_0} \left(\mathbf{J} - \mathbf{J}_{RF} \right) \ , \tag{1}$$

and various heuristic models for the current driven by the applied electric field are used. In the second type of simulations [38, 39], the basic model of Eq. (1) for the driven current is retained, but auxiliary drag/diffusion equation for the RF source is added to model the kinetic equilibration of the RF current:

$$\frac{\partial J_{RF}}{\partial t} = \nabla \cdot (\chi_{\parallel} \nabla_{\parallel} J_{RF}) + \nabla \cdot (\chi_{\perp} \nabla_{\perp} J_{RF}) + \nu (J - J_{RF}) \ . \tag{2}$$

Equation (2) is heuristically derived based on the Fokker-Planck equation [40], and we refer to this model as the Giruzzi model.

Recently, a more rigorous formalism for modeling the inclusion of ECCD sources into the fluid equations has been developed [32]. In addition to the pre-Maxwell equations

$$\nabla \times \mathbf{B} = \mu_0 \mathbf{J} \ , \quad \nabla \cdot \mathbf{B} = 0 \ , \quad \nabla \times \mathbf{E} = -\frac{\partial \mathbf{B}}{\partial t} \ , \tag{3}$$

the equations describing the interaction of MHD with ECRF sources may be written as

$$\frac{\partial \rho}{\partial t} + \nabla \cdot (\rho \mathbf{u}) = 0 \ , \tag{4}$$

$$\rho \frac{\partial \mathbf{u}}{\partial t} + \rho (\mathbf{u} \cdot \nabla) \mathbf{u} = -\nabla p + \mathbf{J} \times \mathbf{B} - \nabla \cdot \overleftrightarrow{\mathbf{\Pi}} + \sum_{\alpha} \mathbf{F}_{\alpha}^{rf} \ , \tag{5}$$

$$\mathbf{E} + \mathbf{u} \times \mathbf{B} = \eta \mathbf{J} + \frac{\mathbf{F}_{e}^{rf}}{n |q_e|} \ , \tag{6}$$

$$\frac{3}{2} n \left(\frac{\partial T}{\partial t} + (\mathbf{u} \cdot \nabla) T \right) + p \nabla \cdot \mathbf{u} = -\nabla \cdot \mathbf{q} - \overleftrightarrow{\mathbf{\Pi}} \colon \nabla \mathbf{u} + Q + \sum_{\alpha} S_{\alpha}^{rf} \ . \tag{7}$$

The variable definitions and details of the various terms are summarized in Appendix A. The RF fields transfer momentum ($\mathbf{F}_\alpha^{rf}$) and energy (S_α^{rf}) to each species of the plasma, and the self–consistent specification of the heat flux $\mathbf{q}$ and the anisotropic stress tensor $\mathbf{\Pi}$ closes the system of equations.

With appropriate closures, this model theoretically captures the full MHD dynamics of the coupled RF/MHD system, including physics traditionally modeled using a Fokker–Planck equation such as the Fisch-Boozer effect [12]. The development of a suitable closure for numerical simulations remains an ongoing research effort, though important theoretical work [32, 41, 42, 43] in the development of self–consistent forms for the fluid equations, the collision/RF operators, and the closures has been carried out. The model also includes the equilibration of the current parallel to the magnetic field lines that is featured in the Giruzzi model. We have chosen not to implement the Giruzzi model; rather, we specify the term in Eq. (6) as

$$\frac{\mathbf{F}_e^{rf}}{n|q_e|} = -\frac{\eta\lambda\mathbf{B}f(\mathbf{x},t)}{\mu_0} \ , \tag{8}$$

wherein λ has units of inverse length and is associated with the ECCD amplitude. The function $f(\mathbf{x},t)$ is dimensionless and stipulates the temporal and spatial (radial, poloidal, and toroidal) localization of RF deposition. In this work, we will use the form

$$f(\mathbf{x},t) = \exp\left(-\frac{(R-R_{rf})^2+(Z-Z_{rf})^2}{w_{rf}^2}\right)\frac{1}{2}\left[\tanh\left(\frac{t-t_o}{t_p}\right)+\tanh\left(\frac{t_o}{t_p}\right)\right] \ . \tag{9}$$

for simplicity. Subscripted quantities are simulation parameters, with w_{rf} denoting the characteristic width ("spot size") about a central deposition point (R_{rf}, Z_{rf}). Following an offset t_o, the time–dependent term ramps up from zero to asymptotically approach unity on a timescale $t_p \ll \tau_R$.

Because we do not directly evolve the RF–induced current according to a Giruzzi model, we first wish to show that we have the physics of RF current equilibration that the latter model includes. The additional term in Eq. (6), which has the form given in Eq. (8), acts as an effective electromotive force and launches both co– and counter–propagating Alfvén waves along the magnetic field lines it intercepts. Assuming such field lines lie in rational surfaces, each wave, after traversing half the closed helical path of the field line, will meet its counterpart, leading to wave superposition on timescales of order the Alfvén time. Nonlinearly the interplay between these waves, along with a small amount of resistive diffusion, yields a local flattening of the parallel current profile $\mu \equiv \mu_0\mathbf{J}\cdot\mathbf{B}/B^2$, which we demonstrate explicitly using the NIMROD code (plasma and code parameters are given in section A). In Figure 1, a computational grid and an axisymmetric equilibrium current distribution (which monotonically decreases toward the plasma edge) are shown for a typical tokamak geometry. NIMROD uses a finite element representation in the poloidal plane, enabling grid packing about the $q = 2$ and $q = 3$ rational surfaces [$q(\psi)$

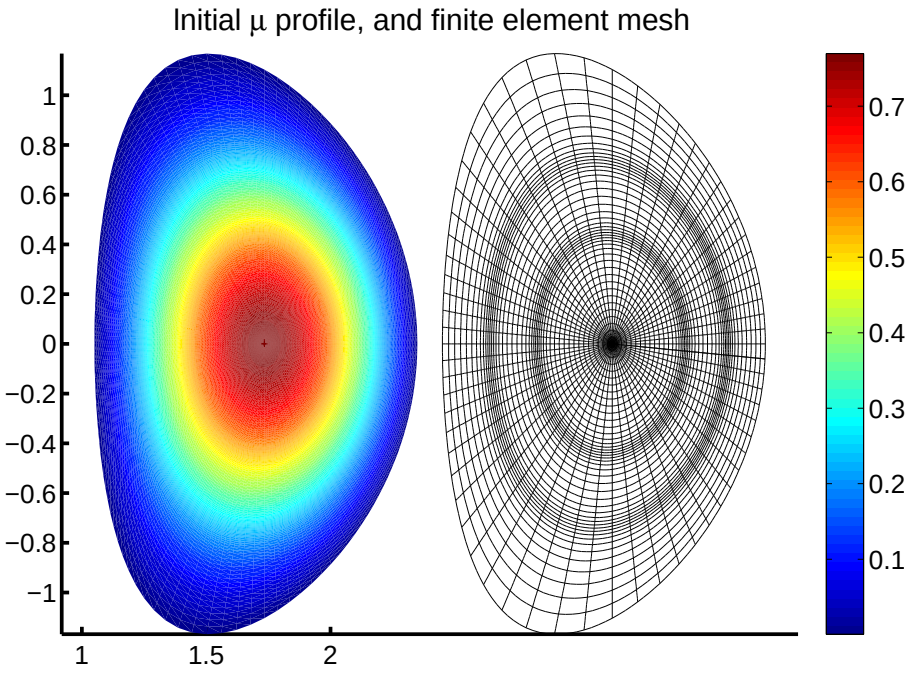

Figure 1: (Color online) The axisymmetric, equilibrium parallel current profile μ for a toroidal plasma, along with the finite element mesh of biquartic elements used to simulate the evolution of the RF/MHD equations in the NIMROD code. Mesh packing is used near the initial positions of the $q = 2$ (inner) and $q = 3$ (outer) rational surfaces.

is shown in Figure 3a]. We restrict the RF source term to be a narrow Gaussian function in the poloidal plane (centered at the $q = 2$ surface on the outboard midplane) and to span only one–tenth of the tokamak's toroidal extent. We then evolve the MHD equations over several thousand Alfvén times and examine the resultant modifications to the μ profile. Figure 2 demonstrates that the profile perturbations indeed have a helical structure consistent with the localization of the RF near the $q = 2$ surface; poloidal cross–sections separated by π radians in the toroidal angle contain μ profiles whose maxima are rotated by $\pi/2$ radians relative to one another. Superposing the perturbations of Figure 2 with the equilibrium profile of Figure 1 shows that the parallel current profile has been locally flattened by the ECCD, along a helical path whose helicity corresponds to the helicity of the rational surface on which the ECCD was injected. At this point in time, a steady-state has not been reached, a point we return to in the

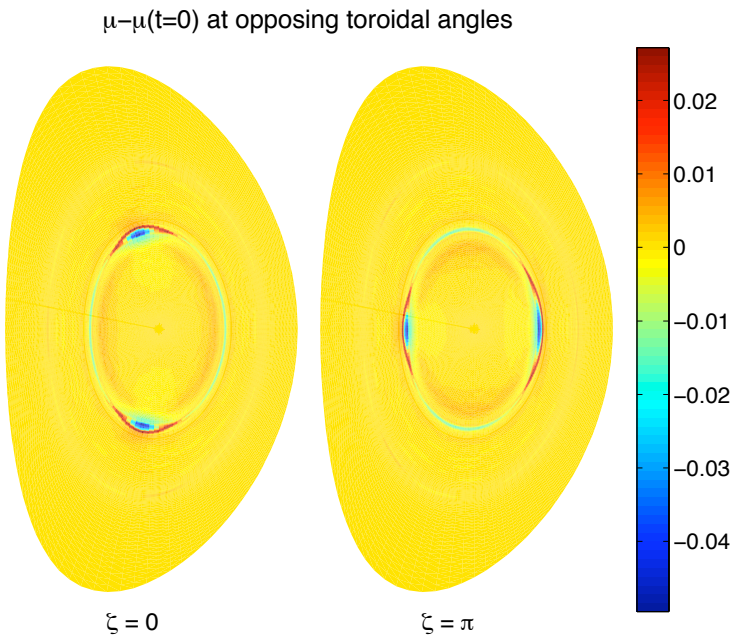

Figure 2: (Color online) In response to a poloidally and toroidally localized RF source, flattening of the μ profile of Figure 1 occurs along a helical path. The RF source is deposited where the $q = 2$ surface meets the outboard midplane, is a Gaussian in the poloidal plane, and spans only one–tenth of the toroidal coordinate ζ.

next section.

Because the direction of wave propagation is parallel to the magnetic field, the timescale for equilibration will be proportional to $k_{\|}$, which goes to zero on the magnetic surfaces and thus varies depending on distance from the rational surface. Although kinetic effects might alter the equilibration times, the relevant time scale is still fast compared to the island growth time, and thus our model accurately calculates the dominant physics of RF equilibration. As well, it retains the dynamics of compressional Alfvén waves, which is absent in simulations using the Giruzzi model (e.g. Ref. [38]) because reduced MHD equations are used. We note that this equilibration is a nonlinear effect of the propagating Alfvén waves, and is thus valid even in the cold plasma limit. Full wave RF codes do not capture this equilibration in the cold plasma limit because they use only linear theory, and the linear cold–plasma dispersion relation does not contain the physics of parallel equilibration.

A The Rutherford equation

The nonlinear growth of magnetic islands generated by tearing modes can be described heuristically by a Rutherford equation [44], appropriately modified to include the neoclassical effects associated with toroidal geometry. Such an equation can be written in the form ([45, 46])

$$\frac{dw}{dt} = \frac{\rho_s^2}{\tau_R}[\Delta' + D_{nc} + D_R + D_{pol} + D_{ECCD} + D_{ECRH}] \ . \tag{10}$$

In this equation, w is the width of the magnetic island, ρ_s is the value of the radial coordinate ρ at the rational surface, and $\tau_R \equiv a^2\mu_0/\eta$ is the conventional resistive diffusion time of the plasma (with a being a representative scale length on the order of the minor radius). The matching index Δ' is the asymptotic matching parameter of tearing mode theory that quantifies the free energy attainable for resistive instability. The subscripted D quantities represent the contribution of various perturbed currents (bootstrap, Pfirsch-Schluter, polarization, and ECCD) and ECRF heating. Because these terms enter additively, we will simplify this study by considering just the modifications resulting from ECCD and neglecting all other terms. A representative Rutherford equation for the study of RF–influenced island growth is then given by

$$\frac{dw}{dt} = \frac{\rho_s^2}{\tau_R}[\Delta'(w) + D_{ECCD}(w)] \ . \tag{11}$$

Though we do not explicitly solve Equation (11), it is instructive to consider the effects of each term. The Δ' parameter is based on the axisymmetric equilibrium current profile and includes the saturation effects [47]. The $D_{ECCD}(w)$ term, which is zero in the limit of zero island size, measures the perturbed helical current inside an island separatrix. Extrapolations of ECCD control and mitigation experiments to ITER–relevant parameters have relied upon analysis and understanding of the terms in the modified Rutherford equation [15, 27] and how they scale. However, a fundamental difficulty is that ECCD influences both terms on the right–hand side of Eq. (11), modifying the Δ' parameter as well as driving perturbed current within the island. Sorting out the effects of both terms independently is difficult, but important if the physics is to be correctly understood.

Using the NIMROD code, we demonstrate the simulation of the nonlinear growth of a tearing mode in the absence of ECCD, and its ability to be described by the Rutherford equation, in Figure 3. The β value for the initial plasma equilibrium is extremely low (of order 10^{-6} near the magnetic axis). The growth of the $n = 1$ Fourier component of the magnetic energy [corresponding to tearing mode growth of a mode with helicity $(m, n) = (2, 1)$] is initially exponential, but is followed by a period of slower growth and saturation. Because the resistive tearing mode obtains its free energy from current profile gradients, the flux–surface average of the parallel current profile μ (denoted $\langle\mu\rangle$) is a useful diagnostic of its long–time behavior. In Figure 4 we demonstrate this effect; the initial $\langle\mu\rangle$ profile (monotonically decreasing toward the plasma edge) undergoes

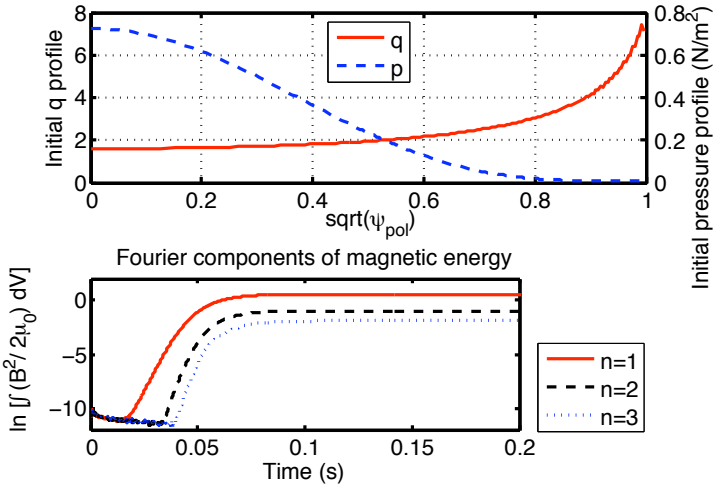

Figure 3: (Color online) (a) The initial $q(\psi)$ and pressure profiles for the toroidal plasmas considered in this work. The equilibrium is unstable to $(m, n) = (2, 1)$ tearing modes at the $q = 2$ rational surface. (b) Time evolution of various Fourier components (corresponding to variation in toroidal angle ξ) of the total magnetic energy as the tearing mode grows. The $n = 1$ component predominates, initially growing exponentially and then saturating; magnetic energy scales with island width w as $E_{mag} \sim w^4$.

a net flattening due to current perturbations near the $q = 2$ rational surface (positioned at the cross in the figure inset) as the tearing mode grows and saturates. Hence, the flattening of the averaged profile near the rational surface can be associated with stability, and additional stabilizing or destabilizing contributions may be expected as ECCD–induced current perturbations locally flatten or steepen this profile further. It should also be noted that the rational surface position is determined (both here and in the remaining sections of this work) by tracing individual field lines in the area of interest and searching for closed helical paths.

We next discuss RF–induced modifications of the plasma's equilibrium current profile, i.e. preemptive Δ' modifications, to prevent island growth.

III Δ' modification in NIMROD

The modification of Δ' by the ECCD is particularly easy to simulate using the NIMROD code [33]. Because NIMROD uses a spectral representation for the toroidal direction, the toroidally symmetric modifications induced by the RF can thus be simulated by initially evolving only the $n = 0$ components until a new equilibrium is reached. Our simulations proceed as follows:

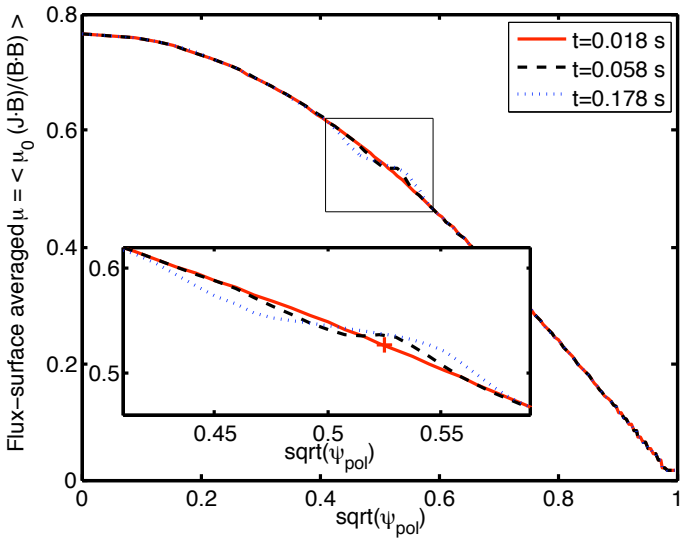

Figure 4: (Color online) Time evolution of the $\langle\mu\rangle$ profile due to the growth and saturation of a tearing mode. The resonant rational surface is initially located at $\sqrt{\psi_{pol}} = 0.525$. (inset) Close–up of the $\langle\mu\rangle$ profile, wherein the rational surface position is denoted by a cross. As the mode saturates (Fig. 3b), a local flattening of the profile is observed near this point, but relatively little motion of the rational surface ensues.

- Begin with an ideally stable, resistive–tearing–mode unstable equilibrium;
- Evolve only the axisymmetric ($n = 0$) Fourier components of the simulation in response to applied electric field (Eq. 9).
- After the new steady–state has been obtained, begin evolving the higher–order Fourier harmonics;
- Measure the observed growth rate to determine the modification of Δ'.

Because the mode growth rate is proportional to a near–unity power of Δ', comparison of the growth rate in the presence or absence of ECCD reveals the influence of the applied RF on this parameter. This approach uses NIMROD's dynamical modeling capability to address the same question posed by Pletzer and Perkins [13], who used the PEST–3 code to calculate Δ' modifications in modified Grad–Shafranov equilibria due to toroidally symmetric, poloidally Gaussian current profiles at or near the mode rational surface.

To reach a new steady-state will take a characteristic time, and it is instructive to consider this time scale not only to understand these simulations, but to understand how this work relates to the dynamic cases we will consider in the next section. The effect of the applied electromotive force introduced by the RF can be best understood by taking the dot product of Eq. (6) with the line

element $d\mathbf{l}$ which traces the path C of a field line in a rational surface. Faraday's law can be used to represent the first term in terms of magnetic flux through the topological surface S bounded by the helical line element C, such that

$$-\int_S \frac{\partial \mathbf{B}}{\partial t} \cdot d\mathbf{A} = \eta \int_C \mathbf{J} \cdot d\mathbf{l} - \frac{\eta\lambda}{\mu_0} \int_C f(\mathbf{x}, t)\mathbf{B} \cdot d\mathbf{l} \ . \tag{12}$$

Equation (12) exhibits the physics of a driven LR circuit, with the first and second terms acting as the inductive and dissipative elements and the last term driving current. The time scale for reaching a steady state is the characteristic L/R time and will depend on the plasma geometry and the plasma resistive time scale $\tau_R = \mu_0 a^2/\eta$, where a is the minor radius of the plasma. If the RF rampup is rapid relative to the latter timescale and remains constant thereafter, curve fits to the normalized, perturbed toroidal plasma current (corresponding to dissipation in the circuit) are well approximated by the form $1 - \exp(t/\tau_{LR})$, where τ_{LR} is the L/R time and has the value $\tau_{LR} \approx 0.22$ s for the simulations in this work. The comparitive resistive time scale is $\tau_R = 1.0$ s for this simulation.

In addition to the parallel equilibration, which occurs on an Alfvénic time scale and reaches steady state on the τ_{LR} time scale, there will be effects from the change of the line element itself. Because the direction of the unit vector $\hat{b}(\mathbf{x}, t)$ is altered by perturbed magnetic fields, the path traversed by solutions of the nonlinear Eq. (12) will vary in space and time, and as the set of such paths constitutes the rational surface, the location of the rational surface will also vary in space and time.

The results of using RF to modify Δ' are shown in Figure 5. The ECCD profiles (with half–width $w_{rf} = 3.7$ cm and centered on the outboard midplane) are shown on the left. The ECCD amplitudes λ for the various datapoints are chosen such that in the long–time limit, the ratio of the ECCD–induced toroidal current I_{RF} to initial toroidal current I_0 (from the equilibrium configuration) ranges from 1–4%. The top right pane of Figure 5 shows the shifted radial position of the $q = 2$ rational surface for various profile locations and amplitudes; the magnitude of the shifts increases as the RF input power is increased. For these shifts, it is instructive to estimate whether the bulk of the RF power is deposited inboard or outboard from the original rational surface position $R_{2,1}(=$ 202.7 cm). This can be done by considering the area under the various profile curves in the left of the figure; the fraction of this area which lies above zero on the y–axis is equivalent to the fraction of RF power deposited outboard from the original rational surface. Radially outward rational surface shifts occur even when upwards of 80% of the RF deposition occurs outside the initial rational surface.

La Haye [22] has noted the critical need for accurate spatial alignment of RF deposition for the mitigation and control of NTMs, and examination of the modified growth rates which result from ECCD–induced alterations of Δ' at long times in our model also affirm the need for accurate spatial alignment of the RF. In the bottom right pane of Figure 5, growth rates are shown which correspond to the various deposition profiles in the left for differing values of the amplitude λ. We will later (Figure 9) show that the saturated $(2, 1)$ island

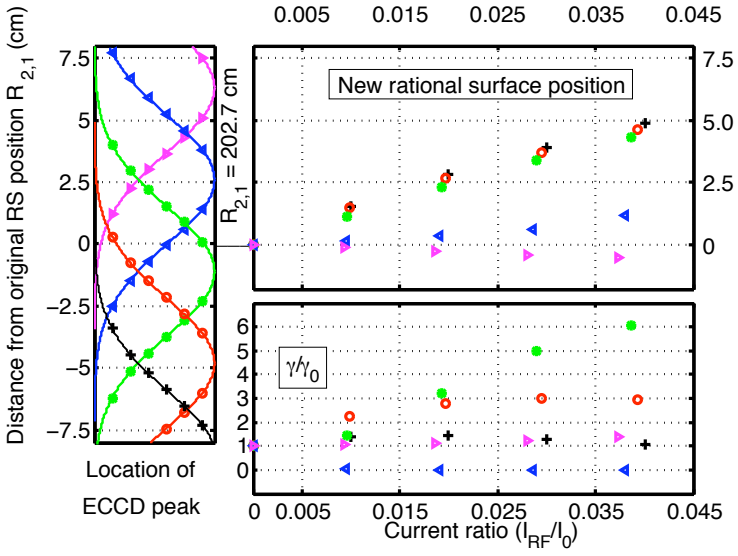

Figure 5: (Color online) (left) On a resistive timescale, ECCD deposition at different input powers and deposition locations shifts the rational surface location relative to its original position, $R_{2,1} = 202.7$ cm. The growth rate of the $(2,1)$ tearing mode, and thus the numerical value of Δ', is also influenced by the input power and location of the ECCD deposition (bottom right).

half–width for this plasma in the absence of RF is $w_0 = 6.5$ cm, and this width can be compared with the quantity $\delta R \equiv R_{rf} - R_{2,1}$, where R_{rf} is the position of the peak ECCD deposition. One observes that relatively minor alterations to the growth rate occur for $|\delta R| \gtrsim w_0$, i.e. for RF depositions which are highly misaligned with the rational surface. The deposition profiles which peak at $\delta R = -8.5$ cm and 6.3 cm are particularly inefficient at mode stabilization because the rational surface has moved in the wrong direction relative to the induced current peak. More notable effects occur for $|\delta R| < w_0$; relevant values are $\delta R = -4.8$ cm, -1.1 cm, and 2.6 cm respectively. For small, negative values of δR, the growth rate of the tearing modes is significantly increased. When δR is small and positive, however, the deposition of RF just outside the rational surface completely stabilizes the tearing mode.

These results are consistent with Figure 6 in the work by Pletzer and Perkins [13], where localized Gaussian current sources ($w_{rf} = 0.03$) cause significant destabilizing effects inside the rational surface but are stabilizing outside. However, interpreting their data in light of rational surface motion and current profile modification provides a more intuitive understanding of their results, since the shift in the position of the rational surface in response to RF injection also has important effects on the stabilization or destabilization of the tearing mode. Consider, for example, the growth rates corresponding to deposition peaked at

$\delta R = 4.8$ cm inboard from the rational surface. Initially these growth rates are increased by low–amplitude RF injection, but increasing the RF amplitude (and thus the current ratio) appears to have little effect on the growth rates for current ratios above 2%. Figure 6 demonstrates the reason for this effect; the RF steepens the $\langle\mu\rangle$ profile just inside the rational surface (leading to instability), but as the RF power is increased, the position of the rational surface is shifted outward away from the profile modifications. Another consequence of this phenomena can be seen in Figure 7, wherein the long–time effects of RF drive peaked at 2.6 cm outside the rational surface stabilize the mode completely at high input powers. Here, the $\langle\mu\rangle$ profile modifications reduce the current gradient at the rational surface, even reversing its direction for high current ratios. However, as the RF power (or, alternatively, the current ratio) is increased, the position of the rational surface is shifted outward. At higher RF powers, as the rational surface crosses the peak of the RF–induced perturbation of $\langle\mu\rangle$, the resulting sign change of the current gradient will yield instability. This effect is conspicuously present in Figure 6 of the work by Pletzer and Perkins (the black diamonds in their plot); the destabilizing effect of RF deposition centered on the rational surface and applied at increasingly high powers arises from the associated outward shift of the rational surface.

These results suggest that Δ' stabilization of the resistive tearing modes in this model exhibits sensitivity not only to the location of the ECCD deposition (as is also the case in experimental efforts to suppress NTMs) but also to the shifts in rational surface position which this deposition induces. Effectively, one is attempting to hit a moving target; the Δ'–stabilizing effect of RF is maximized by highly localized deposition just outside the mode rational surface, but the surface itself also moves in response to the RF perturbation. Nevertheless, we have demonstrated that complete stabilization of the mode is possible, provided that the RF is preemptively applied at the appropriate place and that sufficient time has elapsed for global resistive diffusion of the induced current to occur. We now consider more experimentally relevant effects, namely, the dynamic response of existing islands to the application of ECCD sources.

IV Dynamic response to RF current sources

A ECCD effects on saturated tearing modes

We now wish to determine if the complete stabilization of $(2,1)$ tearing modes at the nonlinear saturation stage can be achieved by the same ECCD injection which, when applied preemptively, modifies Δ' to yield a stable equilibrium. This is one method for determining the relative importance of the $D_{ECCD}(w)$ term of Eq. (11) for an axisymmetric source, since the timescale on which the mode is influenced can be compared to the relevant timescale for Δ' stabilization (τ_{LR}) which we have already examined. We have seen that RF injected just outside the rational surface ($\delta R = 2.6$ cm, in Figure 5) preemptively stabilizes tearing modes at RF input powers $> 1\%$. In Figures 8 and 9, where the current

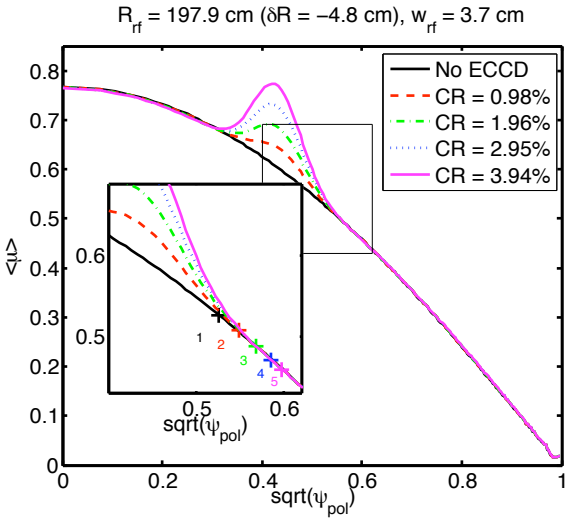

Figure 6: (Color online) Response of the flux–surface averaged μ profile of the plasma to RF sources of increasing current ratio CR $\equiv I_{RF}/I_0$ centered 4.8 cm inward from the original rational surface position. (Inset) Crosses denote the $(2,1)$ rational surface position for each profile, with increasing numbers corresponding to increasing current ratios. Although the RF sources initially steepen the profile near the rational surface (a destabilizing effect), the rational surface position shifts radially outward as the RF power is increased. The steepening cannot persist; further increases in the current ratio exert relatively little influence on the growth rate (as the "o" markers of the bottom right pane of Figure 5 indicate).

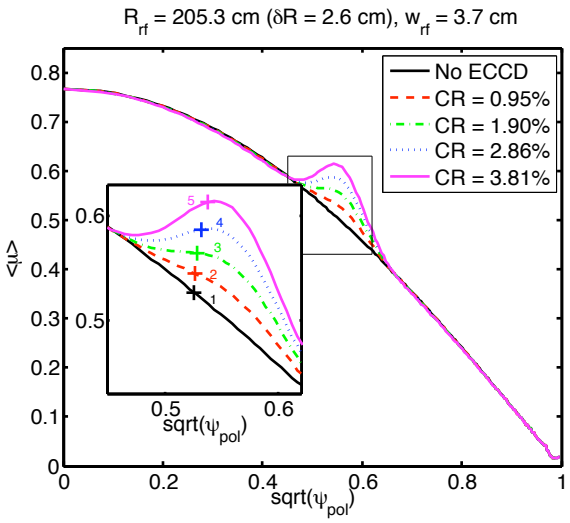

Figure 7: (Color online) Response of the flux–surface averaged μ profile of the plasma to RF sources of increasing current ratio centered 2.6 cm outward from the original rational surface position, with rational surface locations in inset. RF sources initially flatten the profile near the rational surface, yielding a net stabilizing effect. As the current ratio increases, however, the position of the rational surface moves outward toward the RF–induced peak in $\langle\mu\rangle$. Instability will result if the RF power is sufficiently large, due to the change in the local profile gradient as the peak is crossed.

ratio or input power $\delta I_{norm} \equiv I_{RF}(t)/I_{RF}(t=\infty) \approx 3\%$ and 4% for two separate simulations, we apply ECCD at this position subsequent to the growth and saturation of the mode. In Figure 8a, the low–order Fourier components of the total magnetic energy are plotted as the discharge evolves. Initial linear and Rutherford–type growth of the $(2,1)$ magnetic islands raises the $n=1$ magnetic energy to a saturated state at approximately $t = 0.09$ seconds. As the ECCD amplitude begins to rise (see Figure 8b), the value of the magnetic energy (which scales as $E_{mag} \sim w^4$ where w is the island width) begins to decay. As δI_{norm} becomes large, the island width is increasingly reduced. Explicit plots of the saturated $(2,1)$ island structure (~ 13 cm wide) are given in Figure 9a for the 4% current ratio case, and also reveal the presence of $(3,1)$ islands arising from toroidal coupling. Figure 9b, obtained roughly halfway through the discharge, shows that the width of the $(2,1)$ island is reduced in response to the RF and that the $(3,1)$ island has completely vanished. By $t = 0.35$ s, Poincaré plots similar to those of Figure 9 reveal no island structures.

One might expect these simulations to most clearly illustrate the relative importance of the $D_{ECCD}(w)$ term in Eq. (11); because $D_{ECCD}(w)$ is a measure of the amount of current contained within the island, its effect is expected to be most pronounced when current is added while the island is large. However, we observe that the islands are suppressed on a timescale of roughly $0.2 - 0.25$ s $\approx \tau_{LR} = 0.22$, suggesting that Δ' modification remains the dominant stabilization mechanism in these simulations. This behavior is likely related to the relative inefficiency imposed by the toroidally symmetric form of the RF; its intersection with the helical island structure induces currents both favorable and unfavorable to island suppression.

Experimentally, RF current is generally applied while the islands are growing. In the next section, we investigate this more experimentally relevant case, and attempt to determine useful information about the short–time ($t \ll \tau_{LR}$) behavior of Δ' modifications (associated with electric fields and corresponding to the inductive component in the circuit model).

B ECCD effects on growing tearing modes - rational surface response

To examine the short–time effects of applied ECCD on the behavior of growing tearing modes, we repeat the previous simulations without suppressing the $n > 0$ Fourier modes and use an immediate onset time of the RF source (yielding RF–induced rational surface motion before tearing modes begin to grow). We demonstrate this behavior in Figure 10, wherein the vertical axis represents radial distance along the outboard midplane while the horizontal axis represents evolution in time; unlabeled axes signify normalized quantities. In the leftmost plot, the deposition profiles of the (toroidally symmetric) ECCD on the outboard midplane are shown, together with the original position of the rational surface. In the topmost plot, the normalized time variation of the ECCD amplitude and the induced toroidal current are shown, with δI_{norm} again representing the fraction of the total RF–induced toroidal current which has been

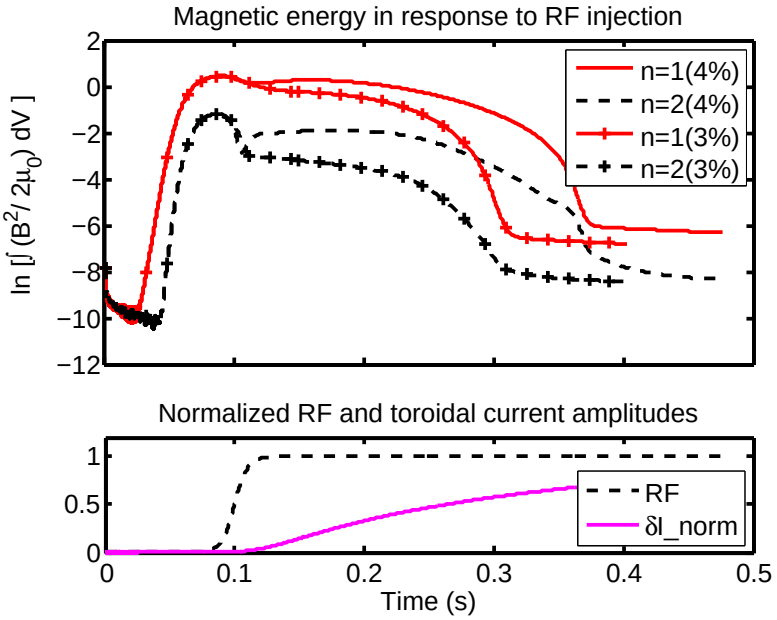

Figure 8: (Color online) (a) Low–order Fourier components of the total magnetic energy for two simulations wherein ECCD sources of different amplitudes are applied to a saturated (2,1) tearing mode. Subsequent to mode saturation, ECCD injection applied on the outboard midplane yields a reduction in the magnetic energy as toroidal current is induced in the plasma. Complete stabilization of the mode is achieved. (b) Behavior of RF amplitude and induced toroidal current (both normalized) in time. Here, δI_{norm} is the fraction of the toroidal current I_{RF} which will ultimately be driven by the ECCD; it is small compared to the equilibrium toroidal current I_0 [$I_{RF}(t=\infty) \approx 0.03 I_0$ or $0.04 I_0$]. Plots of induced current for the two cases overlay one another when normalized; thus, only one is shown.

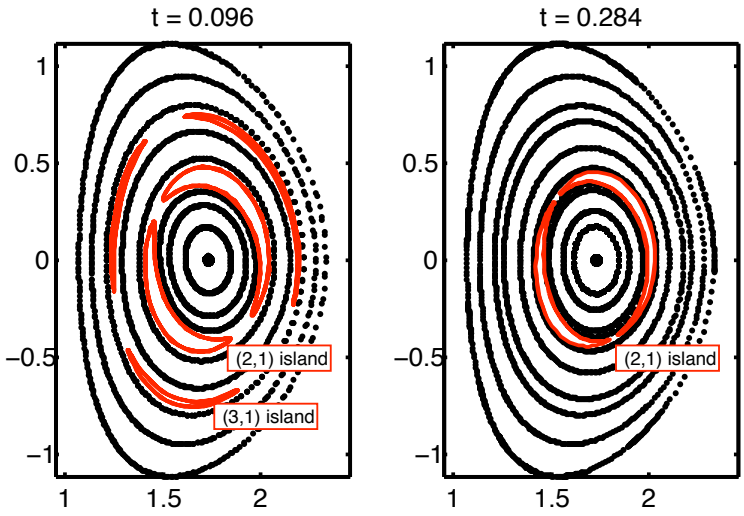

Figure 9: (Color online) Island structure at various points in the discharge of Figure 8 with 4% current ratio. The saturated state of $(2,1)$ and $(3,1)$ magnetic islands, before ECCD is applied, is shown on the left plot. As ECCD is applied these islands are reduced in size (right plot) and ultimately vanish.

induced at a given point in time. Arrangement of the figures in this manner demonstrates the response of the rational surface (found in the largest plot) to both the spatial and temporal behavior of the ECCD. The initial introduction of ECCD induces parallel electric fields in response to the applied electromotive force of the RF, and effectively "pushes" the rational surface away from the region of peak deposition. Thereafter, as the induced current begins to rise, the rational surface position on the outboard midplane moves radially outward with its asymptotic limit being the rightmost set of points in Figure 5. Notably, when ECCD is deposited just outside the rational surface, the initial inward, electric–field dominated motion of the rational surface is countered at longer times by outward, current–induced motion. In addition, characteristics of the short–time growth of the tearing mode in this case can be associated with long–time stability. These signatures of proper ECCD alignment will be discussed further in the next section.

C Numerical experiments - short–time Δ' behavior due to inductive response

To further investigate the effect of short–time ($t \ll \tau_{LR}$) Δ' modification in response to rational surface motion (assuming that the competing D_{ECCD} term in the Rutherford equation plays a minimal role), we follow the procedure used to investigate Δ' modifications in Section III and vary the onset time of the RF source in an effort to separate short–time and long–time effects. We note

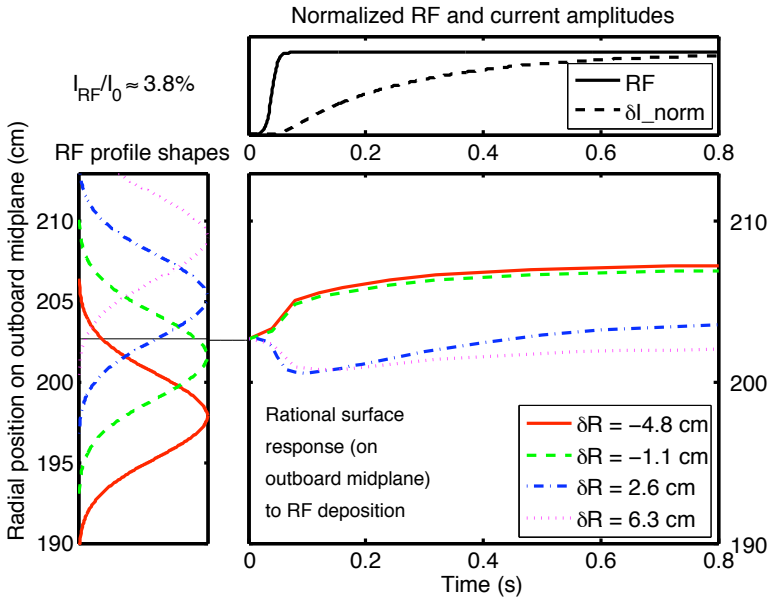

Figure 10: (Color online) (left) Spatial profiles of ECCD deposition centered at various radial locations on the plasma's outboard midplane, in relation to the original position of the $q = 2$ rational surface on the midplane. (top) Temporal behavior of the deposited ECCD profiles and the toroidal current which they induce. (bottom right) Spatiotemporal evolution of the rational surface position in response to ECCD deposition. The initial response of the rational surface is to move away from the peak deposition region. At long times, induced toroidal current moves the surface radially outward.

that this method could also be used to assess the relative contributions from the Δ' and $D_{ECCD}(w)$ terms as the simulation evolves, in cases where the latter term plays a greater role than in the previous section. However, because this $D_{ECCD}(w)$ contributes little to the stabilization even for large islands, we expect that its effects on the linearly growing islands will be minimal in these particular simulations. Our modified procedure is as follows:

- Begin with an ideally stable, resistive–tearing–mode unstable equilibrium;
- Evolve only the axisymmetric ($n = 0$) Fourier components of the simulation in response to ECCD of the form (8) – (9);
- After some characteristic onset time $t_{n>0} \ll \tau_R$, begin evolving the higher–order Fourier harmonics;
- Measure the observed growth rate and compare with other scans.

Stated differently, we are creating a sequence of new axisymmetric equilibria with this form of the RF source, rather than introducing any helical contribu-

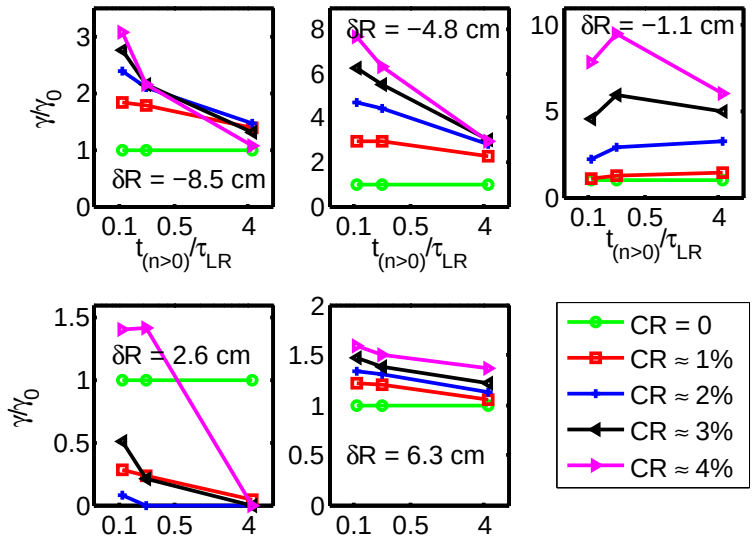

Figure 11: (Color online) Normalized growth rates of the $(2,1)$ tearing mode in response to RF deposition of various powers and locations on the outboard midplane. The $n = 0$ Fourier components of the simulation evolve continuously, while the $n > 0$ components are turned on after various onset times $t_{n>0}$ (normalized to $\tau_{LR} = 0.22$). Growth rates are measured for the various onset times, with the longest value of onset time corresponding to the growth rates obtained in Section III.

tions from the RF. Longer delays before non-axisymmetric components are allowed to evolve can be associated with greater contributions of the steady–state Δ' effects term in the modified Rutherford equation. ECCD–driven current rises to 99% of its peak value in roughly τ_R, which is roughly $4.5\tau_{LR}$; if the onset times $t_{n>0}$ are also on that time scale, the Δ' modifications of Section III will result. For shorter onset times, we expect short–time modifications to Δ' (associated with the inductive, electric field component of the LR circuit model) to dominate. By varying the non-axisymmetric onset time, information about these effects can be separated.

Figure 11 demonstrates the modifications to the tearing mode growth rate observed in these simulations, and includes the long–time Δ' modifications discussed previously (Section III). When alignment with the rational surface is poor, growth rates generally decrease with increasing onset time ($\delta R = -8.5, -4.8, 6.3$ cm), However, they are enhanced relative to the case without ECCD, and this enhancement persists (raising the growth rate by nearly an order of magnitude) when the deposition occurs immediately inboard from the rational surface. However, for $\delta R = 2.6$ cm, wherein the long–time Δ' modifications yield stability or extremely slow growth, low–power RF injection signifi-

cantly reduces the growth rate without fully stabilizing the mode at short times. From this we conclude that the plasma's response to short–time Δ' modifications is rather volatile relative to the long–term effects arising from background profile modification. However, this volatility can also significantly reduce the growth rate of the mode on short timescales when RF alignments are favorable and will ultimately lead to long–term stability of the mode. This reduction can serve as a signature of proper RF alignment, while immediate enhancements to the growth rate suggest that the alignment is poor.

It is also noteworthy that RF current ratios $> 3\%$ (which are stabilizing in the long–time limit) initially act to *destabilize* the mode at short times. Again, the motion of the rational surface is responsible; at short times, the resonant surface is moved radially inward (away from the deposition point which is just outside the rational surface in this case). For adequately large RF amplitudes, the short–time displacement of the surface carries it out of the region where RF effects influence the slope of the current profile and the long–time stability properties. Consequently, attempts to determine proper RF alignment by the method above will be most reliable at low RF input powers; the low power ensures that the short–time displacement of the rational surface will be relatively small.

Returning again to the simulations of Figure 8, in which the ECCD parameters are given by $I_{RF}/I_0 = 0.0286$ or 0.0381, and $\delta R = 2.6$ cm, comparison with the bottom left pane of Figure 11 indicates that the mode growth rate, and thus Δ', is *increased* at short times by the RF deposition for the higher current ratio and *decreased* for the lower current ratio. By $t \approx 0.15$ s in the simulation, this behavior is evident; the saturated mode amplitude for the higher current discharge is slightly elevated relative to its lower–current counterpart. Short–time modifications of Δ', and the associated rational surface motion, may thus prove consequential for mode stabilization. The qualitatively similar responses of both discharges to the increasing toroidal current induced by the RF on the τ_{LR} timescale, however, suggest that contributions from the $D(w)_{ECCD}$ term of Eq. (11) are significant neither at short nor long times for these simulations. This term is expected to play a larger role, however, when toroidally localized RF is applied to saturated islands.

V Summary and conclusions

A simple model for RF stabilization has been implemented in the NIMROD code and used to investigate the effect of ECCD injection on the stability, growth, and dynamical behavior of magnetic islands. The work here does not include a model for the parallel equilibration of the driven current [30]. Because our model uses the full set of inductive equations and includes Faraday's law, unlike the previous reduced MHD simulations [38], an inductive time scale is required for the current to reach a steady state, and not a pure collisional time scale. This results in a slower time scale for our current to reach a steady-state (compare Figure 8 in this paper to Figure 3 in Ref. [38]). While the use of a lower resistivity

in Eq. (8) corresponding to the lower collisionality of fast electrons would yield a faster equilibration time, we have found that Alfvén wave propagation, together with small amounts of dissipation, yields the requisite parallel equilibration on a time scale that is still much faster than the growth time of the mode growth and the ramp times used in the simulations. We expect that once more complete closures for the electron stress tensor are implemented [32, 41, 43], this equilibration time will be even faster (akin to how the Braginskii heat flux closure equilibrates temperature faster than sound waves). For the present work, the correct time scale ordering ensures that the model is valid for our numerical experiments.

This work also differs from Ref. [38] in that a toroidally symmetric electromotive force (induced by RF) was used as a source. In experiments, the dominant toroidal rotation of the island implies the the source will have a finite toroidal width associated with it, even in the case of modulation. Ref. [38] applied a source that was deposited helically, using the justification that the deposition was helical. In this work, we are taking the limit of large rotation and no modulation which corresponds to a toroidally symmetric source. In future work, we will include toroidal localization and finite rotation. In combination with the parallel equilibration physics associated with more complete closures, this will enable more direct comparisons with Ref. [38].

We first tested our model by reproducing the results of Pletzer and Perkins [13]. This test exploits the ability of NIMROD to easily simulate just the axisymmetric evolution of the plasma to reach a new steady state. The optimal position for RF deposition has been verified to be immediately outside the initial rational surface on which the mode grows. The Δ' destabilization at high RF input powers demonstrated by Pletzer and Perkins has been shown to arise from rational surface motion. By explaining features of their data in terms of rational surface movement relative to the parallel current density gradient, we gained experience in analysis which proved useful for explaining subsequent numerical experiments.

We have demonstrated the stabilization of initially saturated tearing modes by the application of toroidally symmetric ECCD at the $(2, 1)$ surface. The timescale for this stabilization has been shown to be approximately equal to τ_{LR}, the L/R time associated with the evolution of RF–induced current perturbations toward a modified, steady–state equilibrium. We conclude that Δ' modification is the dominant stabilization mechanism in this case, even though the RF is applied at a time where the island is large and its intersection with the helical island [as quantified by the $D_{ECCD}(w)$ term] is maximized. In these simulations, the rational surface motion was also shown to be important in interpreting the results; high–power RF injection can, for instance, initially be destabilizing due to rational surface motion even if its long–time behavior yields stability.

We have further examined these ideas by varying the times at which the non-axisymmetric MHD perturbations of the simulations were permitted to evolve. By evolving the $n = 0$ components continuously and varying the onset time of higher–order components, the relative effects of inductive electric fields (on short timescales, $t \ll \tau_{LR}$) were compared with the effects of driven currents arising

on the τ_{LR} timescale. Though the plasma response to Δ' modifications on the former timescale is comparatively more volatile, signatures of favorable RF alignment with the rational surface can be deduced by observing the plasma's response to low–power RF injection on these short timescales. In the latter simulations $D_{ECCD}(w)$ remains relatively unimportant due to the small island size and the relatively low overlap of the toroidally symmetric RF with the helical island.

The use of an axisymmetric RF source in these simulations allowed for simplicity in the analysis and facilitated the study of Δ' effects in isolation. A toroidally-localized RF source should be considerably more effective in contributing to $D_{ECCD}(w)$ stabilization of existing islands on experimentally useful timescales [14]. In future work, we will investigate these effects. However, our model for setting up numerical experiments to determine the relative importance of terms in the Rutherford equation (11) is a useful paradigm. The significance of rational surface motion in response to injected ECCD, both at short and long times, has also been presented. This effect is not easily represented within the modified Rutherford equation, and while alluded to in other papers [13], we have found it necessary to explain the (possibly temporary) destabilization of the tearing modes at higher RF input powers.

This work represents a first step in the development of integrated, predictive models for ECCD/MHD interactions (such as, for example, might be used to determine optimum NTM stabilization approaches in ITER). In the future, we plan to use data from ray tracing codes [48] as the NIMROD simulation progresses to determine the amplitude and spatial localization of the ECCD–induced electromotive forces. In this scenario, NIMROD's magnetic geometry can be exported to the GENRAY and CQL3D codes, which can then calculate ray trajectories and power deposition associated with a particular ECCD configuration. In addition, because these simulations are occuring on the plasma transport time scale, we plan to use more realistic models for plasma heat transport and sources to achieve greater fidelity with experimental observations. One difficulty associated with this type of modeling is that it provides another mechanism for the rational surface to move (in addition to the RF sources discussed above), greatly complicating the simulations. Consequently, we anticipate that accurate calculations of the power required to stabilize islands will require numerical implementation of the same feedback mechanisms which are used in experiments. Relevant examples include the active feedback control systems of DIII-D [23, 24], which induces small variations in the plasma toroidal field or major radius, and of JT-60U [10], which alters the ECCD injection angle.

Effects arising from the development of accurate closure models (which account for the effects of RF on higher–order velocity moments) can also be compared with the results obtained herein to determine the additional physics imparted by the closures. These developments, along with the rigorous verification of self–consistency among collision operators, quasilinear operators, and fluid equations, will serve as future steps of importance in the development of an integrated ECCD/MHD model.

VI Acknowledgements

We wish to thank F. Ebrahimi, J. Carlsson, E. D. Held, J.-Y. Ji, J. D. Callen, R. W. Harvey, A. P. Smirnov, and D. B. Batchelor, as well as members of the SciDAC Center for Extended MHD Modeling (CEMM) and the NIMROD and SWIM teams, for useful discussion and feedback. This work is supported by the SciDAC Center for Simulation of RF Wave Interactions with Magnetohydrodynamics (SWIM), which is funded by the U. S. Department of Energy jointly under the Fusion Energy Sciences and Advanced Scientific Computing Research programs of the Office of Science, via Cooperative Agreement No. DE–FC02–06ER54899. Computations herein were performed primarily at NERSC, which is also supported by the DoE Office of Science under Contract No. DE–AC02–05CH11231.

A The coupled RF/MHD equations

In this section, the relationship of Eqs. (3 - 7) to the more fully self–consistent interaction of RF ECCD injection with MHD [32, 43] is briefly discussed. When localized ECCD is applied, both the distribution function $\tilde{f}_\alpha$ and the fields $\tilde{\mathbf{E}}, \tilde{\mathbf{B}}$ can vary on the rapid timescales associated with the propagation of RF waves through the plasma (we signify such rapid variation with the tilde notation). The dynamics of interest, however, are the slower, self–consistent interaction of fields and distribution functions. To proceed, one averages over a few wave periods of the rapid timescale (denoted $\langle\cdot\rangle_t$) and make a quasilinear approximation [49, 50] for the ECCD effects. The kinetic equation for the averaged distribution function $f_\alpha \equiv \langle\tilde{f}_\alpha\rangle_t$ is then

$$\frac{\partial f_\alpha}{\partial t} + \mathbf{v}\cdot\nabla f_\alpha + \frac{q_\alpha}{m_\alpha}\left[\mathbf{E}(\mathbf{x},t) + \mathbf{v}\times\mathbf{B}(\mathbf{x},t)\right]\cdot\frac{\partial f_\alpha}{\partial \mathbf{v}} = C(f_\alpha) + Q(f_\alpha)\ , \quad \text{(A.1)}$$

where $Q(f_e)$ is the quasilinear operator and contains the physics associated with the rapid oscillation of the electromagnetic fields. The ions are presumed to be unaffected by the RF, i.e. $Q(f_i) = 0$. As velocity moments of the kinetic equation are taken to obtain the fluid equations, we obtain velocity–space integrals over $Q(f_e)$.

The direct integration of Eq. (A.1) over the velocity space yields a continuity equation for the ion and electron fluids. Since ECCD neither creates nor destroys particles in fusion plasmas, the fluid continuity equations, Eq. (4), are unaffected by the RF. The product of $m_\alpha\mathbf{v}$ and the kinetic equation (A.1), when integrated over the velocity space, yields momentum equations for the ion and electron fluids,

$$m_\alpha n_\alpha \frac{\partial \mathbf{u}_\alpha}{\partial t} + m_\alpha n_\alpha(\mathbf{u}_\alpha\cdot\nabla)\mathbf{u}_\alpha = -\nabla p_\alpha - \nabla\cdot\overleftrightarrow{\mathbf{\Pi}}_\alpha + n_\alpha q_\alpha[\mathbf{E}+\mathbf{u}_\alpha\times\mathbf{B}] + \mathbf{R}_\alpha + \mathbf{F}_\alpha^{rf} \quad \text{(A.2)}$$

where the subscripted quantities $n, \mathbf{u}, p, \Pi, \mathbf{R}$, and $\mathbf{F}^{rf}$ are respectively the density, velocity, scalar pressure, anisotropic pressure tensor, and momentum transfer due to collisional friction/RF injection for species α. Summing Eq. (A.2) over species yields an MHD momentum equation, Eq. (5); in addition to the normal terms, the transfer of momentum from RF waves to electrons is also represented. Because of the large mass ratio, however, this additional term is small relative to the ion momentum and is neglected. Assuming an MHD-ordering [51], the electron momentum equation is used to write the generalized Ohm's law as:

$$\mathbf{E} + \mathbf{u} \times \mathbf{B} = \eta \mathbf{J} + \frac{\mathbf{F}_e^{rf}}{n|q_e|} \tag{A.3}$$

where the final term incorporates the RF effects and has the form

$$\mathbf{F}_e^{rf} = \int m_e \mathbf{v} Q(f_e) d^3\mathbf{v} \ . \tag{A.4}$$

This term captures the dominant physics of the ECCD/MHD interaction.

Integration of the product of $m_\alpha(\mathbf{v}-\mathbf{u}_\alpha)\cdot(\mathbf{v}-\mathbf{u}_\alpha)/2$ with the kinetic equation (A.1) yields an equation for the temperature T_α of a given species;

$$\frac{3}{2} n_\alpha \frac{\partial T_\alpha}{\partial t} + \frac{3}{2} n_\alpha (\mathbf{u}_\alpha \cdot \nabla) T_\alpha + n_\alpha T_\alpha \nabla \cdot \mathbf{u}_\alpha = -\nabla \cdot \mathbf{q}_\alpha - \overleftrightarrow{\mathbf{\Pi}}_\alpha \colon [\nabla \mathbf{u}_\alpha] + Q_\alpha + S_\alpha^{rf} \ , \tag{A.5}$$

wherein the subscripted quantities $\mathbf{q}$ and Q represent the heat flux and collisional heating experienced by fluids of species α. Likewise, the RF heating experienced by species α is represented by

$$S_\alpha^{rf} \equiv \int \frac{m_\alpha}{2} (\mathbf{v} - \mathbf{u}_\alpha) \cdot (\mathbf{v} - \mathbf{u}_\alpha) Q(f_\alpha) d^3\mathbf{v} \ . \tag{A.6}$$

Summing this equation over species and dropping small terms yields the standard MHD equation (7) describing the evolution of plasma temperature, as well as a new term representing the effects of localized electron heating imparted by the ECCD. Since our primary focus is to explore the physics of ECCD rather than ECRH, we neglect this term.

A Closures and numerical parameters

The fluid theory closure problem requires the determination of values for heat fluxes ($\mathbf{q}$) and stresses ($\mathbf{\Pi}$) as functions of lower–order fluid moments. In addition to the complexities of the standard closure problem [41], the calculation of a physically consistent closure for our coupled ECCD/MHD model must take into account the presence of the quasilinear RF operator $Q(f_e)$ in the kinetic equation. In this work, we neglect these details and consider simple models for the closure relations. Specifically, we use

$$\mathbf{\Pi} = -\rho\nu\nabla\mathbf{u} \quad \text{(A.7)}$$

$$\mathbf{q} = -\frac{3n}{2}\left[\kappa_\parallel \hat{b}\hat{b} + \kappa_\perp(\mathbf{I} - \hat{b}\hat{b})\right]\cdot\nabla T \quad \text{(A.8)}$$

where $\mathbf{I}$ is the unit tensor, and $\hat{b}$ is the direction of the local magnetic field.

The parameters $\nu, \kappa_\parallel$, and $\kappa_\perp (\ll \kappa_\parallel)$ are the kinematic viscosity and parallel/perpendicular heat diffusivity. In this work, typical values for these parameters are respectively 4.3×10^{-2} m^2/s, 4.3×10^{7} m^2/s, and 4.3×10^{1} m^2/s.

Other parameters relevant to these simulations include the plasma's Lundquist and Prandtl numbers (respectively $S = 1.67 \times 10^6$ and $Pr = 0.1$), the Alfvén and resistive times (respectively $\tau_A \approx 6 \times 10^{-7}$ s and $\tau_R \approx 1.0$ s), the plasma resistivity $\eta/\mu_0 \approx 0.423$ m^2/s, the major radius $R_0 = 1.70$ m, the magnetic field strength at the magnetic axis ($B \approx 1.84$ T) and the poloidal grid resolution (44 radial by 64 axial meshpoints). Fourth–order polynomial interpolation was used within individual finite elements in the poloidal plane.

References

[1] C. C. Hegna, Phys. Plasmas **5**, 1767 (1998).

[2] R. J. La Haye, Phys. Plasmas **13**, 055501 (2006).

[3] H. Zohm, A. Kallenbach, H. Bruhns, G. Fussmann, and O. Klüber, Europhys. Lett. **11**, 745 (1990).

[4] Z. Chang, E. D. Fredrickson, J. D. Callen, K. M. McGuire, M. G. Bell, R. V. Budny, C. E. Bush, D. S. Darrow, A. C. Janos, L. C. Johnson, H. K. Park, S. D. Scott, J. D. Strachan, E. J. Synakowski, G. Taylor, R. M. Wieland, M. C. Zarnstorff, S. J. Zweben, and the TFTR Group, Nucl. Fusion **34**, 1309 (1994).

[5] S. Günter, A. Gude, M. Maraschek, and Q. Yu, Plasma Phys. Controlled Fusion **41**, 767 (1999).

[6] E. J. Strait, L. Lao, A. G. Kellman, T. H. Osborne, R. Snider, R. D. Stambaugh, and T. S. Taylor, Phys. Rev. Lett. **62**, 1282 (1989).

[7] O. Sauter, R. J. La Haye, Z. Chang, D. A. Gates, Y. Kamada, H. Zohm, A. Bondeson, D. Boucher, J. D. Callen, M. S. Chu, T. A. Gianakon, O. Gruber, R. W. Harvey, C. C. Hegna, L. L. Lao, D. A. Monticello, F. Perkins, A. Pletzer, A. H. Reiman, M. Rosenbluth, E. J. Strait, T. S. Taylor, A. D. Turnbull, F. Waelbroeck, J. C. Wesley, H. R. Wilson, and R. Yoshino, Phys. Plasmas **4**, 1654 (1997).

[8] R. J. La Haye, L. L. Lao, E. J. Strait, and T. S. Taylor, Nucl. Fusion **37**, 397 (1997).

[9] R. J. La Haye, B. W. Rice, and E. J. Strait, Nucl. Fusion **40**, 53 (2000).

[10] A. Isayama, Y. Kamada, N. Hayashi, T. Suzuki, T. Oikawa, T. Fujita, T. Fukuda, S. Ide, H. Takenaga, K. Ushigusa, T. Ozeki, Y. Ikeda, N. Umeda, H. Yamada, M. Isobe, Y. Narushima, K. Ikeda, S. Sakakibara, K. Yamazaki, K. Nagasaki and the JT–60 Team, Nucl. Fusion **43**, 1272 (2003).

[11] R. J. La Haye, S. Günter, D. A. Humphreys, J. Lohr, T. C. Luce, M. E. Maraschek, C. C. Petty, R. Prater, J. T. Scoville, and E. J. Strait, Phys. Plasmas **9**, 2051 (2002).

[12] N. J. Fisch, Rev. Mod. Phys. **59**, 175 (1987).

[13] A. Pletzer and F. W. Perkins, Phys. Plasmas **6**, 1589 (1999).

[14] C. C. Hegna and J. D. Callen, Phys. Plasmas **4**, 2940 (1997).

[15] H. Zohm, Phys. Plasmas **4**, 3433 (1997).

[16] H. Zohm, G. Gantenbein, G. Giruzzi, S. Günter, F. Leuterer, M. Maraschek, J. Meskat, A. G. Peeters, W. Suttorp, D. Wagner, M. Zabiégo, ASDEX Upgrade Team, and ECRH Group, Nucl. Fusion **39**, 577 (1999).

[17] G. Gantenbein, H. Zohm, G. Giruzzi, S. Günter, F. Leuterer, M. Maraschek, J. Meskat, Q. Yu, ASDEX Upgrade Team, and ECRH–Group (AUG), Phys. Rev. Lett. **85**, 1242 (2000).

[18] A. Isayama, Y. Kamada, T. Ozeki, S. Ide, T. Fujita, T. Oikawa, T. Suzuki, Y. Neyatani, N. Isei, K. Hamamatsu, Y. Ikeda, K. Takahashi, K. Kajiwara, and the JT–60 Team, Nucl. Fusion **41**, 761 (2001).

[19] C. C. Petty, R. J. La Haye, T. C. Luce, D. A. Humphreys, A. W. Hyatt, J. Lohr, R. Prater, E. J. Strait, and M. R. Wade, Nucl. Fusion **44**, 243 (2004).

[20] H. Zohm, G. Gantenbein, A. Gude, S. Günter, F. Leuterer, M. Maraschek, J. P. Meskat, W. Suttrop, Q. Yu, ASDEX Upgrade Team, and ECRH Group (AUG), Nucl. Fusion **41**, 197 (2001).

[21] M. Maraschek, G. Gantenbein, Q. Yu, H. Zohm, S. Günter, F. Leuterer, A. Manini, ECRH Group, and ASDEX Upgrade Team, Phys. Rev. Lett. **98**, 025005 (2007).

[22] R. J. La Haye, J. R. Ferron, D. A. Humphreys, T. C. Luce, C. C. Petty, R. Prater, E. J. Strait, and A. S. Welander, Nucl. Fusion **48**, 054004 (2008).

[23] R. Prater, R. J. La Haye, J. Lohr, T. C. Luce, C. C. Petty, J. R. Ferron, D. A. Humphreys, E. J. Strait, F. W. Perkins, and R. W. Harvey, Nucl. Fusion **43**, 1128 (2003).

[24] D. A. Humphreys, J. R. Ferron, R. J. La Haye, T. C. Luce, C. C. Petty, R. Prater, and A. S. Welander, Phys. Plasmas **13**, 056113 (2006).

[25] T. C. Hender, D. F. Howell, R. J. Buttery, O. Sauter, F. Sartori, R. J. La Haye, A. W. Hyatt, C. C. Petty, JET EFDA contributors, and the DIII–D team, Nucl. Fusion **44**, 788 (2004).

[26] N. Hayashi, T. Ozeki, K. Hamamatsu, and T. Takizuka, Nucl. Fusion **44**, 477 (2004).

[27] R. J. La Haye, R. Prater, R. J. Buttery, N. Hayashi, A. Isayama, M. E. Maraschek, L. Urso, and H. Zohm, Nucl. Fusion **46**, 451 (2006).

[28] H. Zohm, G. Gantenbein, F. Leuterer, M. Maraschek, E. Poli, L. Urso, and the ASDEX Upgrade Team, Plasma Phys. Control. Fusion **49**, B341 (2007).

[29] The SciDAC Center for Simulation of RF Wave Interactions with Magnetohydrodynamics (SWIM), which funds this work, attempts to address various forms of the general RF/MHD interaction problem through the self–consistent coupling of disparate physics codes. See http://cswim.org for further details.

[30] G. Giruzzi, M. Zabiégo, T. A. Gianakon, X. Garbet, A. Cardinali, S. Bernabei, Nucl. Fusion **39**, 107 (1999).

[31] R. W. Harvey and M. McCoy, *in Proceedings of the IAEA Technical Committee on Simulation and Modeling of Thermonuclear Plasmas* Montreal, Canada, 1992 IAEA, Vienna, 1992, USDOC NTIS Document No. DE93002962.

[32] C. C. Hegna and J. D. Callen, Phys. Plasmas **16**, 112501 (2009).

[33] C. R. Sovinec, A. H. Glasser, T. A. Gianakon, D. C. Barnes, R. A. Nebel, S. E. Kruger, D. D. Schnack, S. J. Plimpton, A. Tarditi, M. S. Chu, and the NIMROD Team, J. Comp. Phys. **195**, 355 (2004).

[34] G. Kurita, T. Tuda, M. Azumi, T. Takizuka, and T. Takeda, Nucl. Fusion **34**, 1497 (1994).

[35] E. Uchimoto, M. Cekic, R. W. Harvey, C. Litwin, S. C. Prager, J. S. Sarff, and C. R. Sovinec, Phys. Plasmas **1**, 3517 (1994).

[36] J. S. Sarff, A. F. Almagri, M. Cekic, C.–S. Chaing, D. Craig, D. J. Den Hartog, G. Fiskel, S. A. Hokin, R. W. Harvey, H. Ji, C. Litwin, S. C. Prager, D. Sinitsyn, C. R. Sovinec, J. C. Sprott, and E. Uchimoto, Phys. Plasmas **2**, 2440 (1995).

[37] C. R. Sovinec and S. C. Prager, Nucl. Fusion **39**, 777 (1999).

[38] Q. Yu, S. Günter, G. Giruzzi, K. Lackner, and M. Zabiego, Phys. Plasmas **7**, 312 (2000).

[39] T. A. Gianakon, Phys. Plasmas **8**, 4105 (2001).

[40] G. Giruzzi, Plasma Phys. Control. Fusion **35**, A123 (1993).

[41] J.-Y. Ji and E. D. Held, Phys. Plasmas **13**, 102013 (2006).

[42] M. Sharma, E. D. Held, and J.-Y. Ji, Bull. APS **53** (abstract only), 39 (2008).

[43] J. J. Ramos, Phys. Plasmas **15**, 082106 (2008).

[44] P. H. Rutherford, Phys. Fluids **16**, 1903 (1973).

[45] O. Sauter, Phys. Plasmas **11**, 4808 (2004).

[46] C. C. Hegna Phys. Plasmas **6**, 3980 (1999).

[47] R. B. White, D. A. Monticello, and M. N. Rosenbluth, Phys. Fluids **20**, 800 (1977).

[48] A. P. Smirnov, R. W. Harvey, and K. Kupfer, Bull. Amer. Phys. Soc. **39**, No. 7, 1626–4R11 (1994).

[49] C. F. Kennel and F. Engelmann, Phys. Fluids **9**, 2377 (1966).

[50] A. N. Kaufman, Phys. Fluids **15**, 1063 (1972).

[51] D. D. Schnack, D. C. Barnes, D. P. Brennan, C. C. Hegna, E. Held, C. C. Kim, S. E. Kruger, A. Y. Pankin, and C. R. Sovinec, Phys. Plasmas **13**, 058103 (2006).